Journal of Power Sources 258 (2014) 246–252

Contents lists available at ScienceDirect

Journal of Power Sources

journal homepage: www.elsevier.com/locate/jpowsour

Short communication

Monodisperse porous $LiFePO_4$/C microspheres derived by microwave-assisted hydrothermal process combined with carbothermal reduction for high power lithium-ion batteries

Rongrong Chen, Yixiong Wu, Xiang Yang Kong*

Institute of Materials for Mobile Energy, School of Materials Science and Engineering, Shanghai Jiao Tong University, Shanghai 200240, PR China

HIGHLIGHTS

- $LiFePO_4$/C microspheres were synthesized through microwave hydrothermal process.
- $LiFePO_4$/C microspheres possess a porous micro/nanostructure and uniform size.
- The high tap density of microspheres can provide a high volumetric energy density.
- Proper amount of carbon coating can improve electronic and ionic conductivities.

GRAPHICAL ABSTRACT

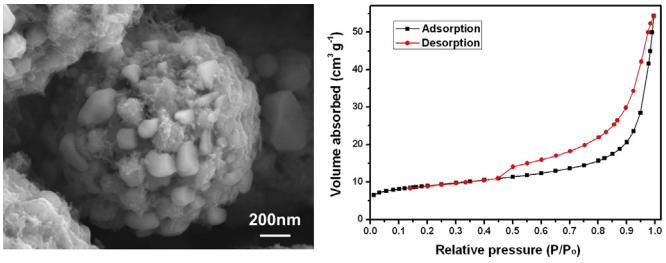

ARTICLE INFO

Article history:
Received 15 December 2013
Received in revised form
22 January 2014
Accepted 19 February 2014
Available online 26 February 2014

Keywords:
$LiFePO_4$/C microspheres
Microwave-assisted hydrothermal process
Carbothermal reduction
Lithium ion batteries

ABSTRACT

A microwave-assisted hydrothermal approach combined with carbothermal reduction has been developed to synthesize monodisperse porous $LiFePO_4$/C microspheres, which possess the diameter range of 1.0–1.5 μm, high tap density of ~1.3 g cm^{-3}, and mesoporous characteristic with Brunauer–Emmett–Teller (BET) surface area of 30.6 m^2 g^{-1}. The obtained microspheres show meatball-like morphology aggregated by the carbon-coated $LiFePO_4$ nanoparticles. The electrochemical impedance spectra (EIS) results indicate that carbon coating can effectively enhance both of the electronic and ionic conductivities for $LiFePO_4$/C microspheres. The Li-ion diffusion coefficient of the $LiFePO_4$/C microspheres calculated from the cyclic voltammetry (CV) curves is ~6.25 × 10^{-9} cm^2 s^{-1}. The electrochemical performance can achieve about 100 and 90 mAh g^{-1} at 5C and 10C charge/discharge rates, respectively. As cathode material, the as-prepared $LiFePO_4$/C microspheres show excellent rate capability and cycle stability, promising for high power lithium-ion batteries.

1. Introduction

Olivine-type lithium iron phosphate $LiFePO_4$, with low cost, nontoxicity, environmental compatibility, excellent chemical stability and safety characteristics, is considered as a promising cathode material for high power lithium-ion batteries [1]. Despite its high theoretical specific capacity (170 mAh g^{-1}) and long cycling lifetime, the rate performance of the original $LiFePO_4$ is significantly restricted by its poor electronic conductivity (~10^{-9} S cm^{-1}) and the slow rate of lithium ion diffusion [2–4]. In the past decade, many groups presented various approaches to improve the rate performance and capacity of $LiFePO_4$ as cathode material. Notably, increasing the electronic conductivity of $LiFePO_4$ by coating with carbon or other conducting layers [5–8], or doping with isovalent

* Corresponding author. Tel.: +86 13916264363.
E-mail address: chenrongchance@sjtu.edu.cn (X.Y. Kong).

http://dx.doi.org/10.1016/j.jpowsour.2014.02.068
0378-7753/

ions [9], becomes a common and effective way for enhancing the rate performance. Moreover, it has also been believed that shortening the Li^+ diffusion distance by decreasing the particle size to 40–200 nm [2,10,11], or making porous morphology through controlling the synthesis conditions [12–16], can improve high power performance. For example, Dominko et al. [12] synthesized porous $LiFePO_4$/C composites with micro-sized particles through sol–gel technique, using ferric citrate, citric acid and lithium dihydrogen phosphate as the source materials. The porous $LiFePO_4$/C composites exhibit good electrochemical performances, over 140 mAh g^{-1} at C/2 rate during continuous cycling. Liu et al. [13] used spray pyrolysis to synthesize 3D nanoporous spherical $LiFePO_4$/C material. The 3D conductive carbon coating and interconnected pore networks facilitated the kinetics of both electron transport and lithium ion diffusion within the particles, which is responsible for excellent cyclability and superior rate capability. However, these reported porous spherical $LiFePO_4$/C materials perform low tap density of around 0.80–0.90 g cm^{-3}. It is well-known that the tap density is also a significant property for electrode materials in lithium-ion batteries since it reflects the volumetric energy density of resulted electrodes [16]. Micro/nanostructured $LiFePO_4$ microspheres with close-packed arrays were suggested for improving the tap density and volumetric energy density of the electrodes [14,16]. Sun et al. [14] developed a novel solvothermal approach combined with high-temperature calcinations to synthesize $LiFePO_4$ microspheres consisting of nanoplates with an open three-dimensional porous microstructure. These micro/nanostructured $LiFePO_4$ microspheres had a high tap density of ~1.1 g cm^{-3}, and exhibited excellent rate capability and cycle stability. Oh et al. [7,16] synthesized double carbon-coated $LiFePO_4$ particles with micrometer size derived by co-precipitation and calcination, performing high tap density of 1.5 g cm^{-3}. The as-received $LiFePO_4$ cathode exhibits high gravimetric and volumetric capacities at high currents owing to the combined effect of the spongelike porous morphology and the double carbon-coating. However, these two methods mentioned above cost long time of reaction, and the starting materials, such as iron (III) nitrate hydrate adapted as the iron source, are not environmental friendly.

To date, numerous synthetic strategies have been developed to prepare $LiFePO_4$, including hydrothermal [17], solvothermal [2,18], co-precipitation [19], sol–gel [12,20], and microwave hydrothermal process [5,10]. In this work, we employed a microwave-assisted hydrothermal approach combined with carbothermal reduction to synthesize monodisperse porous $LiFePO_4$/C microspheres. The environmentally friendly ferric citrate and lithium dihydrogen phosphate are adapted as starting materials. The obtained microspheres show meatball-like morphology aggregated by the carbon-coated $LiFePO_4$ nanoparticles. The $LiFePO_4$/C microspheres also perform uniform size, high tap density, and excellent electrochemical performance.

2. Experimental

2.1. Synthesis of $LiFePO_4$/C microspheres

Monodisperse porous $LiFePO_4$/C microspheres were synthesized through a microwave-assisted hydrothermal process combined with carbothermal reduction. In a typical synthetic condition, 0.015 mol of lithium dihydrogen phosphate (LiH_2PO_4, 99%, aladdin) and 0.0138 mol of ferric citrate ($C_6H_5FeO_7$, AR, Shanghai Chemical Reagents Corporation) with Fe/Li in the molar ratio of 0.92:1 were dissolved into 30 ml of deionized water by continuously stirring at 80 °C. After 30 min magnetic stirring, a yellow solution with pH value of 3 was obtained. This reaction solution was transferred into a 50 ml Teflon vessel, sealed, and heated at 200 °C for 20 min in a commercial microwave reaction apparatus (MDS-6, Shanghai Sineo Microwave Chemistry Technology Co.). The obtained slurry was naturally cooled to room temperature and directly dried in vacuum at 80 °C overnight to get a green precursor. The precursor was reground together with 4 wt% or 8 wt% sucrose as additional carbon source for carbothermal reduction. The as-received samples are termed as LFP-C4 and LFP-C8, respectively. For a comparison, the original precursor without adding sucrose was also calcined, termed as LFP-C0. The carbothermal reductions were conducted at 700 °C under Ar/2 vol.% H_2 atmosphere for 2 h with a heating rate of 5 °C per minute.

2.2. Physical characterization of $LiFePO_4$/C microspheres

The carbon contents of the final products were measured by high frequency infrared ray carbon sulphur analyser (CSI, Baoying, CS-206). The phase and morphology were characterized by X-ray diffraction (XRD, Rigaku Ultima IV, Japan) using Cu Kα radiation and scanning electron microscopy (SEM, Zeiss ULTRA 55, Germany), respectively. Elemental mapping was obtained using an Oxford INCA EDS detector. TEM images and selected-area electron diffraction (SAED) were carried out with a JEM 2100F transmission electron microscope (JEOL, Japan) with an acceleration voltage of 200 kV. Brunauer–Emmett–Teller (BET) measurements were carried out on an ASAP 2020 M surface area & porosity analyzer (Micromeritics, USA). To measure the tap density, 5 g $LiFePO_4$/C product was placed in a 5 ml measuring cylinder and tapped for at least 10 min. The measured volume of the tapped powder and its mass were used to calculate the tap density of the as-prepared samples.

2.3. Cell fabrication and electrochemical measurements

Electrochemical performances of the obtained materials were evaluated by standard CR2025 coin cells. The cathode film was prepared from a mixture of active material ($LiFePO_4$/C), acetylene black (Shanghai Chemical Reagents Corporation) and polyvinylidene fluoride (PVDF, Shanghai Chemical Reagents Corporation) (80:10:10 wt%) with an area of 1.13 cm^2. Metallic lithium foil was used as the anode electrode; a Celgard 2325 membrane served as the separator; the electrolyte was 1 M $LiPF_6$ in a 1:1 solvent mixture of ethylene carbonate (EC)/dimethyl carbonate (DMC). The

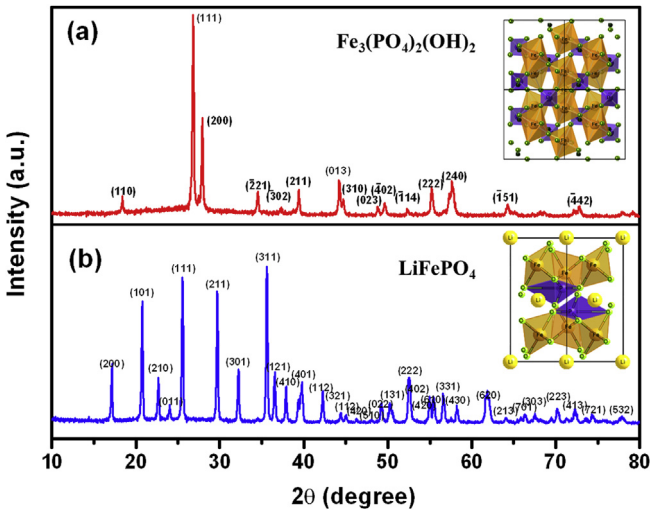

Fig. 1. XRD patterns of (a) $Fe_3(PO_4)_2(OH)_2$ microspheres and (b) $LiFePO_4$/C microspheres.

cells were assembled in an argon-filled glove box (M Braun, Germany), and then were aged for 12 h before charge/discharge to ensure full absorption of the electrolyte into the electrode. Charge–discharge performances were evaluated at 2.0–4.3 V with a Land-CT2001A battery test system (Jinnuo Wuhan Corp., China). The cyclic voltammetry (CV) and electrochemical impedance spectra (EIS) were performed with an electrochemical workstation (Solartron Modulab, UK).

3. Results and discussion

The precursors derived by microwave-assisted hydrothermal reaction and the final products subjected to carbothermal reduction were both examined by XRD for identifying the phase structures. Fig. 1a shows a typical XRD pattern of the as-synthesized precursor, the main peaks are well consistent with the standard $Fe_3(PO_4)_2(OH)_2$ (JCPDS No. 33-0668). And XRD pattern of the final product shown in Fig. 1b can be indexed as the standard orthorhombic $LiFePO_4$ (JCPDS No. 83-2092) with the unit parameters (a = 10.329 Å, b = 6.011 Å, c = 4.693 Å). The diffraction peaks are strong and narrow without any detectable impurity phases, indicating the high crystallinity of the $LiFePO_4$/C sample. The carbon contents of the final products with different amount of sucrose added in carbothermal reduction process were examined by CSI. The carbon contents of LFP-C0, LFP-C4 and LFP-C8 samples are 3.95, 6.69 and 9.17 wt%, respectively.

The morphologies of the as-received samples were observed by scanning electron microscopy (SEM). Fig. 2a and c illustrates the morphologies of $Fe_3(PO_4)_2(OH)_2$ precursor, showing the uniform meatball-like microspheres with diameters of 1.0–1.5 μm aggregated by nanoparticles. SEM images of $LiFePO_4$/C microspheres are shown in Fig. 2b and d. It can be observed that the meatball-like morphology retained after the carbothermal reduction, and $LiFePO_4$/C microspheres are composed of carbon-coated nanoparticles with size of 50–150 nm. The morphologies of the $Fe_3(PO_4)_2(OH)_2$ precursor and $LiFePO_4$/C microspheres were further

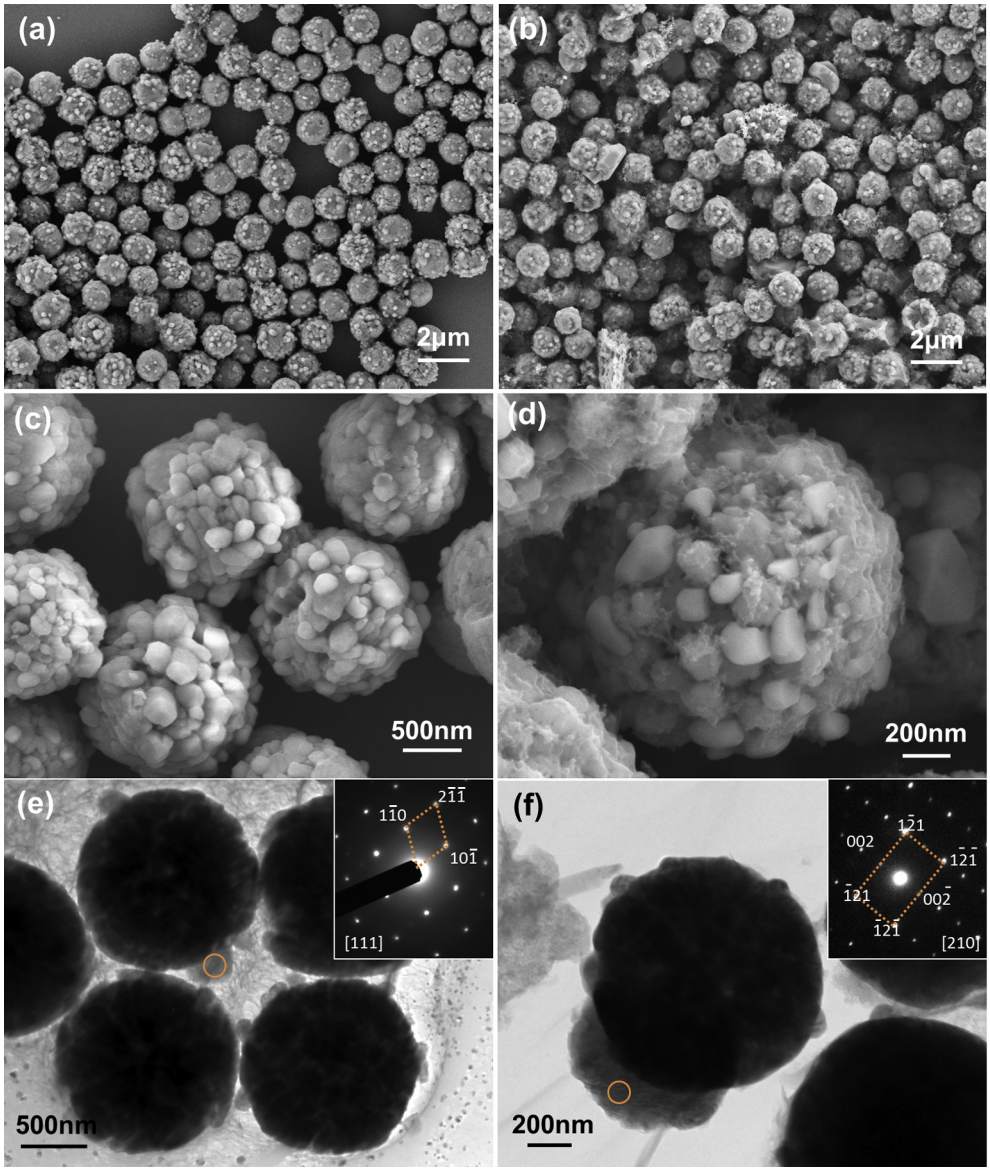

Fig. 2. SEM images of (a, c) $Fe_3(PO_4)_2(OH)_2$ microspheres and (b, d) $LiFePO_4$/C microspheres; TEM images of (e) $Fe_3(PO_4)_2(OH)_2$ and (f) $LiFePO_4$/C microspheres as well as the corresponding SAED patterns (the insets).

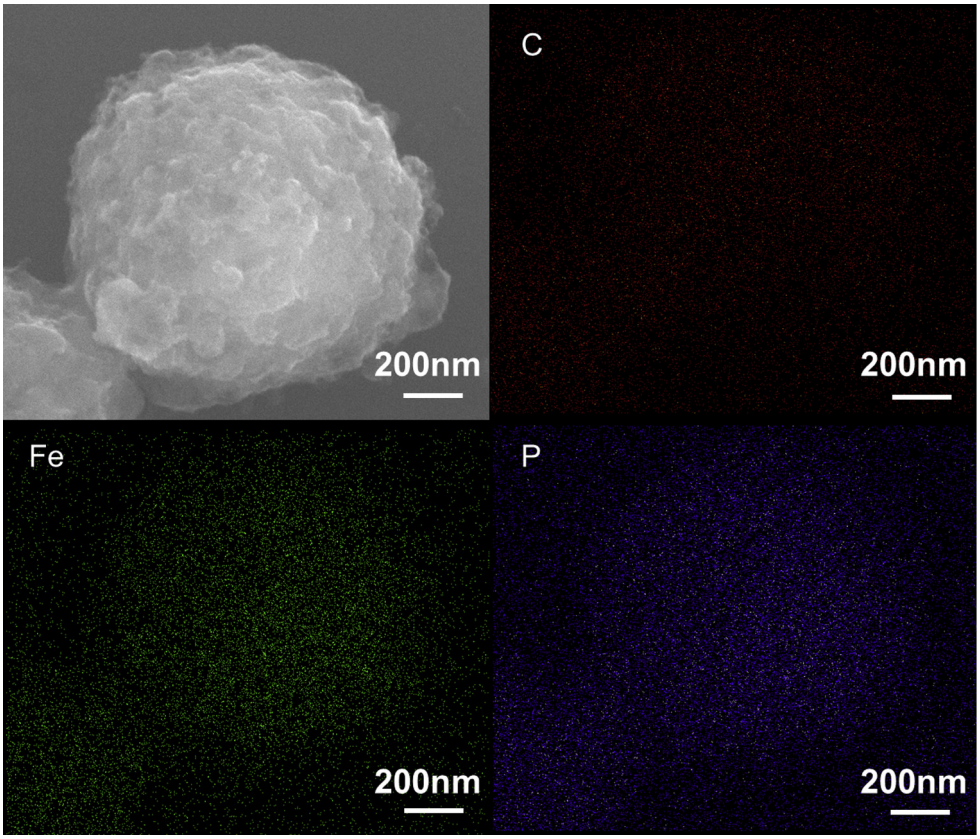

Fig. 3. EDS mappings of Fe, P, C from an individual $LiFePO_4$/C microsphere.

characterized by TEM, as shown in Fig. 2e and f, respectively. From these bright field images, it is clear that both these two kind of microspheres show porous morphology aggregated by nanoparticles. The inserted SAED patterns in Fig. 2e and f were recorded from the rims of microspheres. The sharp refraction spots indicate both of the nanoparticles from $Fe_3(PO_4)_2(OH)_2$ precursor and $LiFePO_4$/C microspheres are single crystals. The SAED pattern in Fig. 2e can be indexed as the zone axis of [111] direction from the monoclinic structure of $Fe_3(PO_4)_2(OH)_2$, and the pattern in Fig. 2f is identified as the zone axis of [210] direction from the orthorhombic structure of $LiFePO_4$, which are consistent with the XRD results. The chemical composition of $LiFePO_4$/C microspheres was examined by EDS. Elemental mapping of EDS was recorded from a typical porous $LiFePO_4$/C microsphere, shown in Fig. 3. The distributions of Fe and P are quite uniform; C is also well distributed over all surfaces, suggesting that $LiFePO_4$ nanoparticles are surrounded by well-interconnected conducting network.

As seen in the cross-sectional SEM image (Fig. 4a, inset) of a typical $LiFePO_4$/C microsphere, there are nanopores in the microsphere extending from the surface to the inner parts of the spheres, which can facilitate deep penetration of liquid electrolyte into the microspheres, thus providing more interface area between the electrode material and the electrolyte. Fig. 4 shows the nitrogen adsorption–desorption isotherm and the corresponding

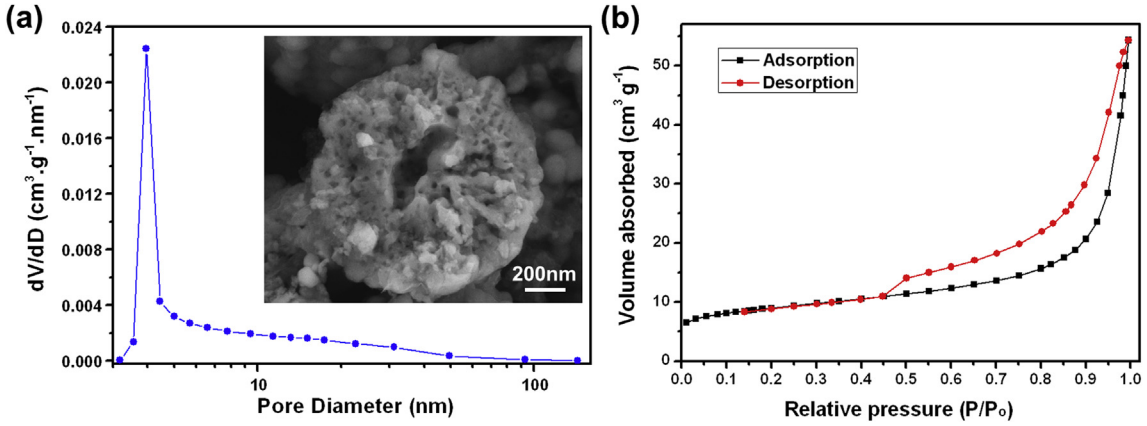

Fig. 4. (a) Barret–Joyner–Halenda (BJH) pore size distribution curves of $LiFePO_4$/C microspheres and high-magnification SEM image of cross-section of a single $LiFePO_4$/C microsphere, (b) nitrogen adsorption and desorption isotherms of $LiFePO_4$/C microspheres.

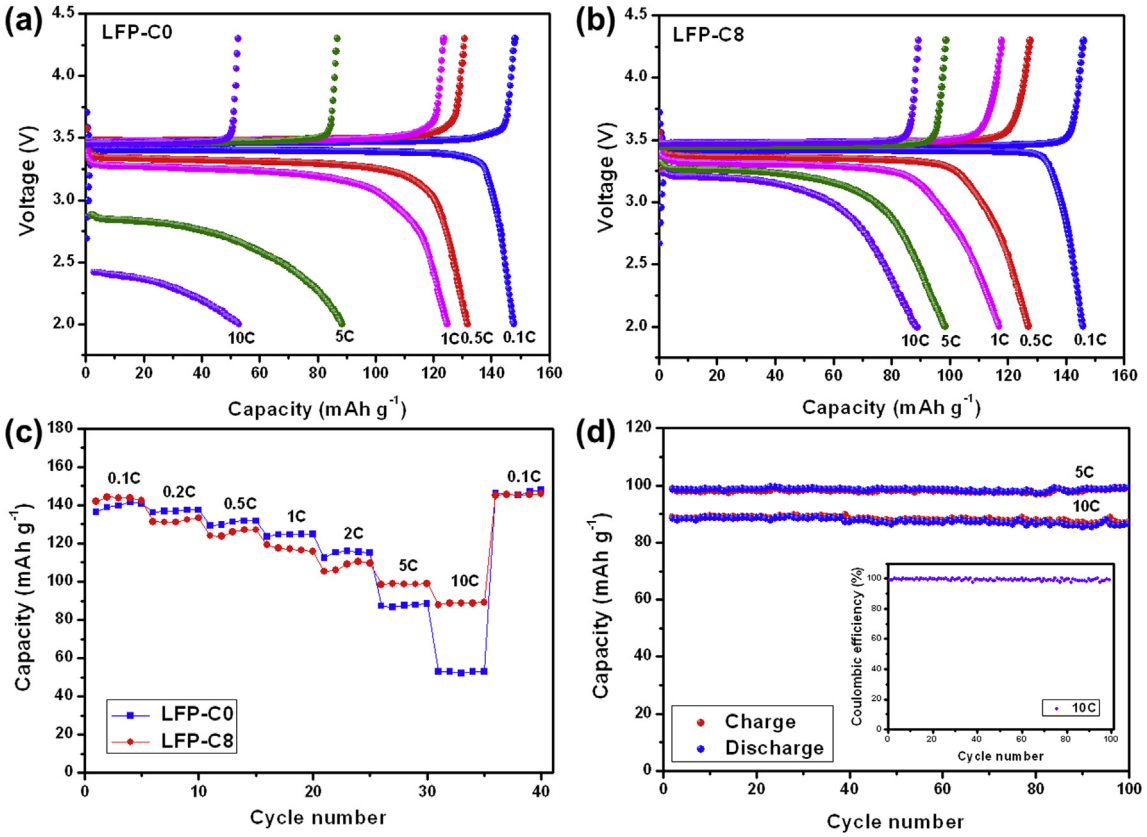

Fig. 5. Charge/discharge curves at various rates of (a) LFP-C0 and (b) LFP-C8 electrodes, (c) discharge capacities at various rates of LFP-C0 and LFP-C8 electrodes, and (d) cycling performances of LFP-C8 electrode at 5C and 10C.

Barret–Joyner–Halenda (BJH) pore size distribution curves of the as-synthesized $LiFePO_4$/C microspheres. The adsorption isotherm shows a type IV curve with an H3 hysteresis loop, indicating a mesoporous characteristic [21]. The measured Brunauer–Emmett–Teller (BET) area is 30.6 $m^2\ g^{-1}$. The average pore diameter is 11.6 nm, calculated from the desorption branch of the nitrogen isotherm with the BJH method. The measured tap density of the as-synthesized $LiFePO_4$/C microspheres with different carbon content is ranged from 1.2 to 1.3 g cm^{-3}, much higher than the maximum value of ~1.0 g cm^{-3} measured from nano-sized individual $LiFePO_4$ particles [14]. The as-prepared meatball-like microspheres allow a much tighter packing of the nanoparticles than the nano-sized individual particles, hence providing much higher volumetric capacity than that of the nano-$LiFePO_4$ materials.

The electrochemical performances of $LiFePO_4$/C microspheres with different carbon contents were examined by means of testing half coin cells. For a typical comparison, the samples of LFP-C0 and LFP-C8 microspheres were employed as the cathodes, and Fig. 5a and b shows the charge/discharge curves at various discharge rates from 0.1C to 10C. Both the LFP-C0 and LFP-C8 microspheres exhibit high specific discharge capacities at 0.1C charge/discharge rate, 148 mAh g^{-1} and 146 mAh g^{-1} (corresponding to 154 and 160 mAh g^{-1} of pure $LiFePO_4$, about 90% and 94% of the theoretical capacity of 170 mAh g^{-1}) respectively. The rate performances of the

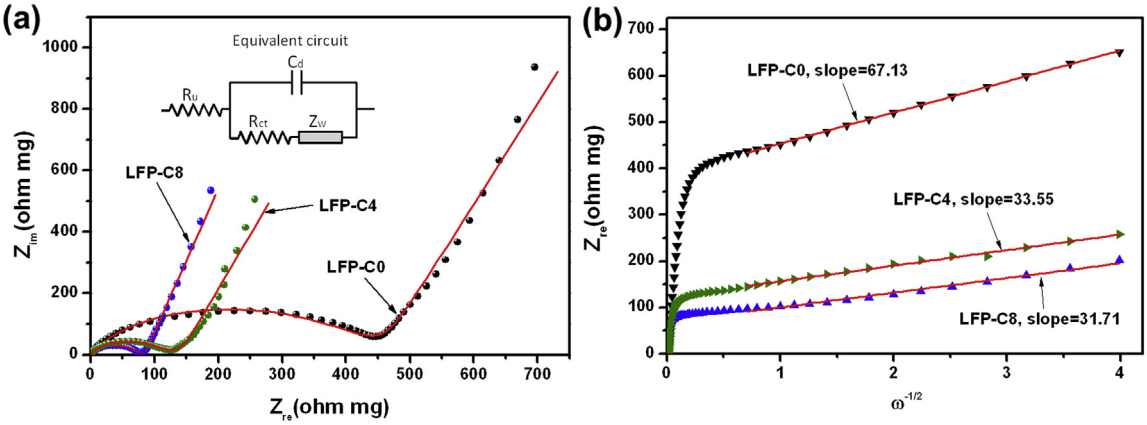

Fig. 6. (a) Impedance spectra recorded in the frequency range of 100 kHz to 10 mHz of LFP-C0, LFP-C4, and LFP-C8 electrodes, and (b) linear fitting of Warburg impedance.

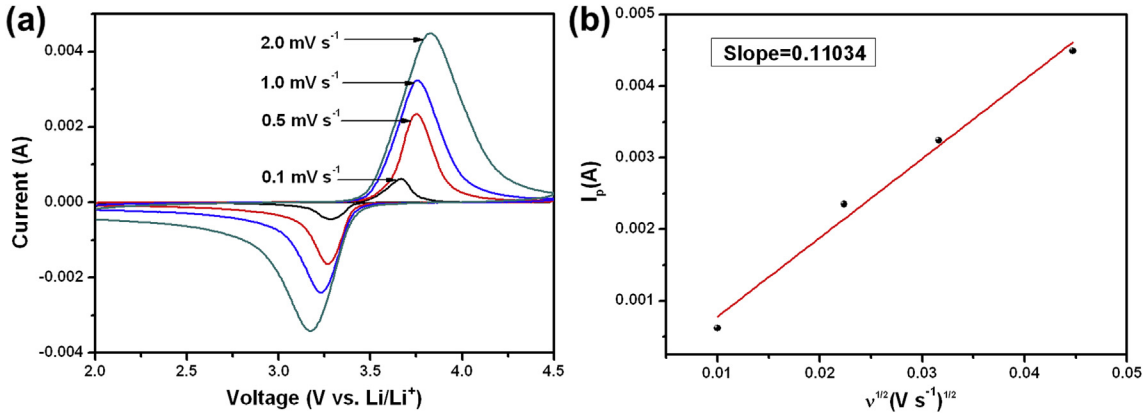

Fig. 7. (a) CV curves of LFP-C8 electrode at scanning rates from 0.1 mV s^{-1} to 2.0 mV s^{-1}, and (b) slope of I_p vs $v^{1/2}$ line.

LFP-C0 and LFP-C8 electrodes are shown in Fig. 5c. The capacity difference between LFP-C0 and LFP-C8 electrode is unremarkable at charge/discharge rates from 0.1C to 2C. In contrast, the rate capacities of LFP-C8 respectively reach 100 and 90 mAh g^{-1} at 5C and 10C charge/discharge rates, much better than those of LFP-C0 microspheres. To evaluate the cycling performance of the LFP-C8 microspheres, full charge/discharge cycles at constant 5C and 10C rates were pursued, as shown in Fig. 5d. The cyclability of LFP-C8 cathode material was very stable during extensive cycling at high current density (1700 mAh g^{-1}, 10C); the capacity retention over 100 cycles is 98% and the average coulombic efficiency is 99%, implying the possibility of high power applications.

Fig. 6a compares the electrochemical impedance spectra (EIS) of the synthesized LFP-C0, LFP-C4 and LFP-C8 electrodes. The impedance spectra can be explained on the basis of an equivalent circuit (as shown in the inset of Fig. 6a) with uncompensated resistance (R_u), charge transfer resistance (R_{ct}), double-layer capacitance (C_d), and Warburg impedance (Z_w) [5,22]. The high-frequency intercept of the semicircle refers to the uncompensated resistance (R_u), and the diameter of the semicircle refers to the charge transfer resistance (R_{ct}). R_u includes the particle–particle contact resistance, electrolyte resistance, and the resistance between the electrode and the current collector. R_{ct} is related to the electrochemical reaction at the electrode–electrolyte interface and particle–particle contact [23]. It can be seen that the charge-transfer resistance decreases from ~410 Ω mg in LFP-C0 to ~72 Ω mg in LFP-C8, indicating the enhanced electronic conductivity due to the additional carbon coating. The inclined lines in the low frequency range are attributed to the Warburg impedance (Z_w), which is associated with the lithium-ion diffusion in the electrodes. The Warburg coefficient (A_w) equals to the slope of Z_{re}–$\omega^{-1/2}$ line under low frequency, ω is the angular frequency of alternating current (AC). As revealed in Fig. 6b, the Warburg coefficients (A_w) of LFP-C0, LFP-C4 and LFP-C8 are respectively 67.13, 33.55 and 31.71, confirming that the additional carbon coating helps increase the ionic conductivity as well.

Fig. 7a shows the cyclic voltammetry result of LFP-C8 electrode at scanning rates from 0.1 to 2.0 mV s^{-1} after activation at a scan rate of 0.5 mV s^{-1} for one cycle. The symmetry of the sharp oxidation and reduction peaks in the CV curves confirms the good reversibility of lithium extraction/insertion reactions in LFP-C8 material. The peak currents I_p (Amperes) at different sweep rates can be used to calculate Li-ion diffusion coefficient D (cm^2 s^{-1}), according to the Randles Sevcik equation [2]: $I_p = 2.69 \times 10^5 A C D^{1/2} n^{3/2} v^{1/2}$, where A is the electrode area (cm^2), C is the concentration of the species being oxidized or reduced (mol cm^{-3}), n is the number of electrons transferred ($n = 1$ for Fe^{2+}/Fe^{3+} redox pair), and v is the potential scan rate (V s^{-1}). As shown in Fig. 7b, the Li-ion diffusion coefficient of LFP-C8 electrode is ~6.25×10^{-9} cm^2 s^{-1}, calculated from the slope of the line. This result illustrates that the Li ion diffusion coefficient of the LFP-C8 microspheres is as good as the nano-sized $LiFePO_4$ materials reported before [2].

4. Conclusions

In summary, we have developed a microwave-assisted hydrothermal approach combined with carbothermal reduction to synthesize monodisperse porous $LiFePO_4$/C microspheres with meatball-like morphology aggregated by carbon-coated $LiFePO_4$ nanoparticles. The environmentally friendly ferric citrate and lithium dihydrogen phosphate are adapted as starting materials. Proper amount of carbon coating can effectively enhance both of the electronic and ionic conductivities for $LiFePO_4$/C microspheres, hence improving the rate capability and cycle stability as cathode material. Due to its high tap density, the $LiFePO_4$/C microspheres can provide high volumetric energy density as well as excellent electrochemical performance as cathode material, promising for high power lithium-ion batteries.

Acknowledgments

This work was supported by the Shanghai Municipal Science and Technology Commission under Grant No. 11JC1405600, and research Fund for the Doctoral Program of Higher Education of China under Grant No. 20120073110008.

References

[1] A.K. Padhi, K.S. Nanjundaswamy, J.B. Goodenough, J. Electrochem. Soc. 144 (1997) 1188–1194.
[2] S. Yang, X. Zhou, J. Zhang, Z. Liu, J. Mater. Chem. 20 (2010) 8086–8091.
[3] M.S. Islam, D.J. Driscoll, C.A.J. Fisher, P.R. Slater, Chem. Mater. 17 (2005) 5085–5092.
[4] Y.N. Xu, S.Y. Chung, J.T. Bloking, Y.M. Chiang, W.Y. Ching, Electrochem. Solid-State Lett. 7 (2004) A131–A134.
[5] A. Vadivel Murugan, T. Muraliganth, A. Manthiram, J. Electrochem. Soc. 156 (2009) A79–A83.
[6] R. Dominko, M. Gaberscek, J. Drofenik, M. Bele, S. Pejovnik, J. Jamnik, J. Power Sources 119–121 (2003) 770–773.
[7] S.W. Oh, S.T. Myung, S.M. Oh, K.H. Oh, K. Amine, B. Scrosati, Y.K. Sun, Adv. Mater. 22 (2010) 4842–4845.
[8] G.M. Song, Y. Wu, Q. Xu, G. Liu, J. Power Sources 195 (2010) 3913–3917.
[9] C. Wang, J. Hong, Electrochem. Solid-State Lett. 10 (2007) A65–A69.
[10] A. Vadivel Murugan, T. Muraliganth, A. Manthiram, J. Phys. Chem. C 112 (2008) 14665–14671.
[11] P. Gibot, M. Casas-Cabanas, L. Laffont, S. Levasseur, P. Carlach, S. Hamelet, J.M. Tarascon, C. Masquelier, Nat. Mater. 7 (2008) 741–747.

[12] R. Dominko, M. Bele, M. Gaberscek, M. Remskar, D. Hanzel, J.M. Goupil, S. Pejovnik, J. Jamnik, J. Power Sources 153 (2006) 274–280.
[13] J. Liu, T.E. Conry, X. Song, M.M. Doeff, T.J. Richardson, Energy Environ. Sci. 4 (2011) 885–888.
[14] C. Sun, S. Rajasekhara, J.B. Goodenough, F. Zhou, J. Am. Chem. Soc. 133 (2011) 2132–2135.
[15] J. Yang, J. Wang, D. Wang, X. Li, D. Geng, G. Liang, M. Gauthier, R. Li, X. Sun, J. Power Sources 208 (2012) 340–344.
[16] S.W. Oh, S.T. Myung, H.J. Bang, C.S. Yoon, K. Amine, Y.K. Sun, Electrochem. Solid-State Lett. 12 (2009) A181–A185.
[17] B. Pei, H. Yao, W. Zhang, Z. Yang, J. Power Sources 220 (2012) 317–323.
[18] Y. Zhang, W. Wang, P. Li, Y. Fu, X. Ma, J. Power Sources 210 (2012) 47–53.
[19] S. Wang, H. Yang, L. Feng, S. Sun, J. Guo, Y. Yang, H. Wei, J. Power Sources 233 (2013) 43–46.
[20] S. Beninati, L. Damen, M. Mastragostino, J. Power Sources 194 (2009) 1094–1098.
[21] K.S.W. Sing, D.H. Everett, R.A.W. Haul, L. Moscou, R.A. Pierotti, J. Rouquerol, T. Siemieniewska, Pure Appl. Chem. 57 (1985) 603–619.
[22] H.C. Shin, W.I. Cho, H. Jang, Electrochim. Acta 52 (2006) 1472–1476.
[23] Y.M. Choi, S.I. Pyun, Solid State Ionics 99 (1997) 173–183.